Generation of an axially super-resolved quasi-spherical focal spot using an amplitude-modulated radially polarized beam

Han Lin, Baohua Jia, and Min Gu*

Centre for Micro-Photonics and CUDOS, Faculty of Engineering and Industrial Sciences, Swinburne University of Technology, P.O. Box 218, Hawthorn, Victoria 3122, Australia
**Corresponding author: mgu@swin.edu.au*

Received April 13, 2011; accepted May 16, 2011;
posted May 27, 2011 (Doc. ID 145874); published June 22, 2011

An axially super-resolved quasi-spherical focal spot can be generated by focusing an amplitude-modulated radially polarized beam through a high numerical aperture objective. A method based on the unique depolarization properties of a circular focus is proposed to design the amplitude modulation. The generated focal spot shows a ratio of $x:y:z = 1:1:1.48$ for the normalized FWHM in three dimensions, compared to that of $x:y:z = 1:0.74:1.72$ under linear polarization (in the x direction) illumination. Moreover, the focusable light efficiency of the designed amplitude-modulated beam is 65%, which is more than 3 times higher than the optimized case under linear polarization and thus make the amplitude-modulated radial polarization beam more suitable for a wide range of applications.

OCIS codes: 050.1970, 220.1230.

Achieving a higher axial resolution and overcoming the axial elongation of a point spread function (PSF) of an objective have remained a fundamental challenge for confocal microscopy, three-dimensional (3D) laser nanofabrication, and optical data storage. Several methods based on the linearly polarized incidence, such as using the 4Pi microscope [1], shaded-ring filters [2,3], and purely absorbing or complex transmittance pupils in confocal scanning microscopy [4,5], have been proposed to enhance the axial resolution of the PSF. Among them, using a shaded-ring filter to modulate the amplitude distribution is preferred, since it does not lead to undesired strong sidelobes. However, the focusable light efficiency of the optimized shaded-ring filter for a linearly polarized beam [2,3] is low (<20%). Moreover, the inherent elongated field distribution associated with a linearly polarized beam in the focal plane along the incident polarization direction makes it impossible to achieve a circular focal spot even when the axial size of the PSF is optimized.

Because of the circular symmetry in the focal plane of a radially polarized beam and the flexibility to manipulate the three polarization components in the focal region [6–9], radially polarized beams have found broad applications in laser trapping [10], nanorod excitation [11], 3D laser nanofabrication [12], plasmonic lensing [13], and the generation of a longitudinally polarized focal spot [14,15]. In this Letter, we propose and demonstrate both theoretically and experimentally the use of an amplitude-modulated radially polarized beam for generating an axially super-resolved quasi-spherical focal spot through manipulating the radial and longitudinal polarization components in the focal region. Compared with the optimized design under linear polarization illumination [2,3], the amplitude-modulated radially polarized beam can not only maintain the transverse circular symmetry of the focal spot but also provide an improvement of the focusable energy by a factor of 3. Compared with the unmodulated focal spot under radial polarization illumination, a 34% improvement in the axial/transverse aspect ratio and an 18.5% enhancement in axial resolution have been achieved.

An amplitude-modulated radially polarized beam can be generated using the setup shown in Fig. 1(a), in which a spatial light modulator (SLM) and a radial polarization converter are employed. Our method starts by considering the incidence of a monochromatic, radially polarized uniform plane wave on the back aperture of an aberration-free high NA objective obeying the sine condition shown in Fig. 1(b). According to the vectorial Debye theory [16], the electric fields of the longitudinal component E_z and radial component E_r in the focal region are given as

$$E_z(r,z) = \int_0^{\theta_{\max}} P(\theta)(1-\cos(2\theta))J_0(nkr\sin\theta) \times \exp(inkz\cos\theta)\mathrm{d}\theta, \quad (1)$$

$$E_r(r,z) = \int_0^{\theta_{\max}} P(\theta)\sin(2\theta)J_1(nkr\sin\theta) \times \exp(inkz\cos\theta)\mathrm{d}\theta, \quad (2)$$

where $P(\theta) = P(R)\sqrt{\cos\theta}$ is the apodization function of the focusing objective, $P(R)$ is the amplitude distribution within the lens aperture, and R is the coordinates in the aperture plane. $\theta_{\max} = a\sin(\mathrm{NA}/n)$ is the maximum value of the convergence angle θ. In this Letter, the NA is 1.4 and n is 1.514. k is the wavenumber of the incident beam, and r and z are the coordinates in the focal region as defined in Fig. 1(b). f is the focal length of the objective. $J_0(x)$ and $J_1(x)$ are the zeroth-order and the first-order Bessel functions of the first kind.

From the Bessel function J_0 in the integral given by Eq. (1), one can see that a key feature of the focal field of a radially polarized beam is the existence of a strong and axially elongated longitudinal component that has its peak on the optical axis. Meanwhile, the radial component has a donut shape with a zero field strength on

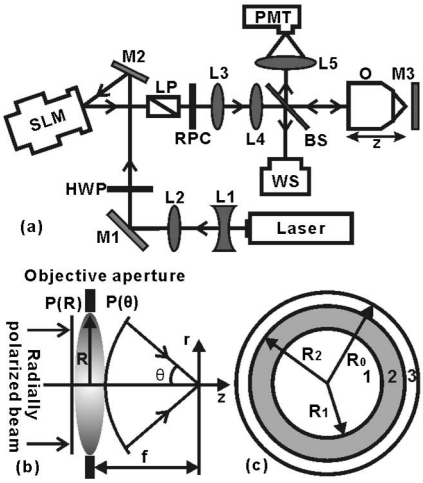

Fig. 1. (a) Schematic of experiment setup of an SLM-assisted confocal microscope system under radially polarized beam illumination. L, lens; M, mirror; HWP, half-wave plate; LP, linear polarizer; RPC, radial polarization converter; WS, wavefront sensor; BS, beam splitter; O, objective (NA = 1.4). (b) Schematic of a radially polarized wave focused by a high NA objective. (c) Schematic of a three-zone amplitude modulation pattern.

the optical axis, owing to the Bessel function J_1 in the integral given by Eq. (2). Thus the axial resolution solely depends on the longitudinal component, which is dominantly contributed by the large convergence angle portion of the incident beam. For the radial direction, since the size of the radial component, which is dominantly controlled by the small convergence angle portion of the incident beam, is much larger than that of the longitudinal component, it would be beneficial if the strength of the radial component and the longitudinal component could be balanced, which leads to a quasi-spherical overall focal spot. Based on these analyses, a three-zone amplitude-modulated back aperture is designed, as shown in Fig. 1(c), to manipulate the weighting of the two vectorial components in the focal region so that the aspect ratio and axial resolution of the PSF can be engineered. In the design, the transparent zone 1 and zone 3 dominantly contribute to the radial and longitudinal components, respectively. The semitransparent zone 2 is used to control the weighting of these two components through the tuning of the transmittance. R_1 and R_2 are the normalized radii of zone 1 and zone 2 to the objective aperture, respectively.

To characterize the focal spot, we define the following parameters. The aspect ratio is defined as $\alpha = W_z/W_r$, where W_z is the FWHM in the axial direction and W_r is the FWHM in the radial direction. The enhancement in axial resolution is defined as $\beta = W_{z0}/W_z$, where W_{z0} is the normalized axial size (normalized to the wavelength of the incident beam at 800 nm) of an unmodulated radial focus. The ratio of the sidelobe strength compared to that of the central lobe is defined as $\varepsilon = I_{s\max}/I_{c\max}$, where $I_{s\max}$ is the peak intensity of the highest sidelobe and $I_{c\max}$ is the peak intensity of the central lobe. The focusable light efficiency of the amplitude modulation is defined as $\eta = A_m/A_0$, where A_m and A_0 are the integrals of modulated field amplitude and the field amplitude of a uniform plane wave across the pupil aperture, respectively. Our aims are (a) to enhance the axial resolution ($\beta > 1$), (b) to achieve a quasi-spherical focal spot (α close to 1), (c) to achieve high focusable light efficiency ($\eta > 60\%$), and (d) to suppress the sidelobes ($\varepsilon \le 0.3$). In the following, we present a case design of the amplitude-modulated radially polarized beam to fulfill all the requirements mentioned above.

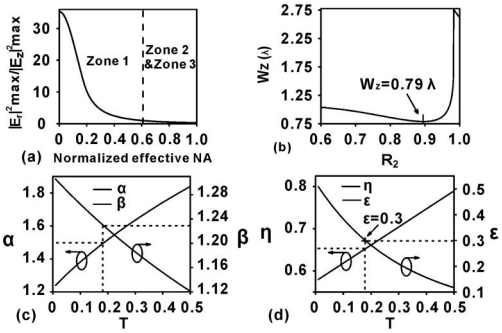

Fig. 2. (a) Ratio of the peak intensity of the radial and longitudinal components versus the normalized effective NA. The dashed line marks $|E_r|^2_{\max} = |E_z|^2_{\max}$ when the effective NA is 0.61. (b) The axial size W_z of the focal spot versus R_2. (c) Dependence of the aspect ratio (α) and the axial resolution enhancement (β) on the transmission of zone 2 (T). (d) Dependence of the focusable light efficiency (η) and the ratio of sidelobe strength (ε) on the transmission of zone 2 (T).

We first optimize R_1 without considering the high angle contributions from zone 2 and zone 3 to maximize the contributions to the radial component, which effectively corresponds to the reduction of the NA of the objective. The dependence of the ratio of the radial and longitudinal peak intensities on the effective NA is shown in Fig. 2(a). It is found that the radial component has a strength equal to the longitudinal component when the effective NA is 0.61, which can be used as the boundary radius for zone 1 as shown in Fig. 2(a).

Under this condition, high angle incident light in zone 3 can be optimized by considering zone 1 is transparent and zone 2 is opaque to increase the effective NA so that enhanced axial resolution can be achieved. The normalized FWHM in the axial direction W_z versus R_2 is shown in Fig. 2(b). The smallest size is 0.79λ, occurring at $R_2 = 0.89$ for the 1.4 NA objective. The transmission of zone 2 is adjusted to control the weighting of the radial and longitudinal components, which eventually control the aspect ratio (α), axial resolution enhancement (β), sidelobe strength (ε) of the focal spot, and transmission efficiency (η). The dependence of α, β, ε, and η on the transmission (T) of zone 2 is shown in Figs. 2(c) and 2(d).

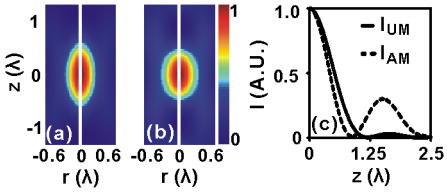

Fig. 3. (Color online) (a), (b) Calculated electric field density distributions in the focus for unmodulated and amplitude-modulated radially polarized beams. (c) Cross sections of the focal spots in the axial direction as marked in (a) and (b) with the white lines. r and z are coordinates normalized by the wavelength of the incident beam.

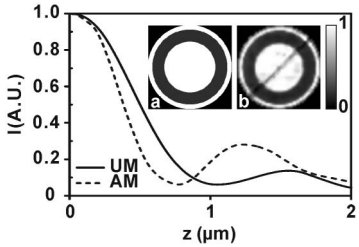

Fig. 4. Measured axial responses for unmodulated (UM) and amplidute-modulated (AM) radially polarized beams. Inset a: Designed amplitude modulation pattern. Inset b: Measured intensity distribution of the generated amplitude modulation measured by a wavefront sensor.

As expected, the light from zone 2 contributes more to the longitudinal component than the radial component. Increasing the transmission of zone 2 enlarges the aspect ratio due to the increase in the strength and the axial size of the longitudinal component. At the same time, the focusable light efficiency is improved and the sidelobe strength is decreased. Since $\varepsilon \le 0.3$ is a reasonably low sidelobe [2], it has been used as one of the criteria for our design. Under such a circumstance the corresponding transmittance is $T = 0.18$, the aspect ratio is 1.48, the axial resolution enhancement is 1.23, and the overall focusable light efficiency is 65%, as marked in Fig. 2, compared with the unmodulated radially polarized beam. Therefore, the normalized amplitude distribution function of the designed beam is

$$P(R) = \begin{cases} 1 & R \le R_1 \\ 0.18 & R_1 \le R \le R_2 \\ 1 & R_2 \le R \le R_0 \end{cases}.$$

The electric energy density profiles of the total field in the focal region of a radially polarized uniform beam and the one with the designed amplitude modulation, focused by a 1.4 NA objective, are presented in Figs. 3(a) and 3(b), respectively. An improvement of 34% in the aspect ratio is evident. At the same time an 18.5% improvement in axial resolution can be also achieved, which is shown in the cross-section comparison in Fig. 3(c). The result can also be compared to the optimized shaded-ring filter designed for a linearly x-polarized beam. The 3D FWHM ratio is $x:y:z = 1:1:1.48$ in our case, while $x:y:z = 1:0.74:1.72$ in the optimized linear polarization case. Most important of all, the energy transmission efficiency of our design is 65%, which is more than 3 times that of the optimized shaded-ring filter [2,3].

Using the experiment setup shown in Fig. 1(a), we experimentally verified our design. The amplitude modulation of a femtosecond laser beam at wavelength 800 nm is generated using an SLM (Holoeye Pluto) based on the birefringence of the liquid-crystal molecules [17]. This amplidute-modulated beam is converted to a radial polarization state through a radial polarization converter (Arcopix) [18]. The gray-level image of the designed amplitude modulation and the generated beam amplitude profile measured by a wavefront sensor (HASO) are shown in insets a and b of Fig. 4, respectively, which are almost identical except the dark line in the middle, which is introduced by the phase singularities of the radial polarization converter [17]. The axial response of the focused beam by a high NA objective (Olympus, UPLSAPO 100×, 1.40 NA) from a gold coated mirror (M3) is recorded by a photomultiplier tube (PMT). The experimental axial response curves, which are average results of ten time measurements, reproduce the shape of the theoretical calculation in Fig. 3(c). The FWHM of the axial response of the unmodulated focal spot is 935 ± 5 nm, while the one with the amplitude modulation pattern is 760 ± 5 nm. An 18.5% enhancement is achieved, matching the theoretical prediction exactly.

In conclusion, we have demonstrated both theoretically and experimentally a design of the amplitude-modulated radially polarized beam for generating an axially super-resolved quasi-spherical focal spot. Based on controlling the weighting of the radial and longitudinal components in the focal region, we have obtained a 34% improvement in the aspect ratio and an 18.5% enhancement in axial resolution. Compared to the optimized shaded-ring filter designed for a linearly x-polarized beam, we have achieved 16% and 58% improvements in the aspect ratio in the x–z and y–z planes, respectively. Moreover, the focusable light efficiency of the designed amplitude-modulated radially polarized beam is more than 3 times higher.

This work is produced with the assistance of the Australian Research Council (ARC) under the Centres of Excellence Program. CUDOS (the Centre for Ultra-high-bandwidth Devices for Optical Systems) is an ARC Centre of Excellence. B. Jia is supported by the ARC Australia postdoctoral fellowship (APD) grant DP0987006. The authors acknowledge the helpful discussion with M. D. Turner and H. Kang.

References

1. C. M. Blanca, J. Bewersdorf, and S. W. Hell, Appl. Phys. Lett. **79**, 2321 (2001).
2. M. Martínez-Corral, C. Ibáñez-López, G. Saavedra, and M. T. Caballero, Opt. Express **11**, 1740 (2003).
3. C. Ibáñez-López, G. Saavedra, and G. Boyer, Opt. Express **13**, 6168 (2005).
4. Z. Ding, G. Wang, M. Gu, Z. Wang, and Z. Fan, Appl. Opt. **36**, 360 (1997).
5. C. J. R. Sheppard, Opt. Lett. **24**, 505 (1999).
6. R. Dorn, S. Quabis, and G. Leuchs, Phys. Rev. Lett. **91**, 233901 (2003).
7. Q. Zhan, Adv. Opt. Photon. **1**, 1 (2009).
8. H. Kang, B. Jia, and M. Gu, Opt. Express **18**, 10813 (2010).
9. M. T. Caballero, C. Ibáñez-López, and M. Martínez-Corral, Opt. Eng. **45**, 098003 (2006).
10. Q. Zhan, Opt. Express **12**, 3377 (2004).
11. H. Kang, B. Jia, J. Li, D. Morrish, and M. Gu, Appl. Phys. Lett. **96**, 065702 (2010).
12. B. Jia, H. Kang, J. Li, and M. Gu, Opt. Lett. **34**, 1918 (2009).
13. W. Chen, D. C. Abeysinghe, R. L. Nelson, and Q. Zhan, Nano Lett. **9**, 4320 (2009).
14. H. Wang, L. Shi, B. Lukyanchuk, C. Sheppard, and C. T. Chong, Nat. Photonics **2**, 501 (2008).
15. K. Huang, P. Shi, X. Kang, X. Zhang, and Y. Li, Opt. Lett. **35**, 965 (2010).
16. M. Gu, *Advanced Optical Imaging Theory* (Springer, 1999).
17. N. Fukuchi, Y. E. Biqing, Y. Igasaki, N. Yoshida, Y. Kobayashi, and T. Hara, Opt. Rev. **12**, 372 (2005).
18. Http://www.arcoptix.com/.